Priority Report

Quantitative Assessment of the p53–Mdm2 Feedback Loop Using Protein Lysate Microarrays

Sundhar Ramalingam[1], Peter Honkanen[2], Lynn Young[3], Tsutomu Shimura[4], John Austin[2], Patricia S. Steeg[1,4] and Satoshi Nishizuka[1,5]

[1]Molecular Therapeutics Program, [4]Laboratory of Molecular Pharmacology, National Cancer Institute, [3]Center for Information Technology, National Institutes of Health, Bethesda, MD 20892; [2]Aushon BioSystems, Burlington, MA 01803; and [5]Laboratory of Proteomics and Analytical Technologies, Research Technology Program, SAIC-Frederick, Inc., National Cancer Institute at Frederick, Frederick, MD 21702.

Requests for reprints: Satoshi Nishizuka, Molecular Therapeutics Program, National Cancer Institute, National Institutes of Health, 9000 Rockville Pike, Bethesda, MD 20892. Fax: 301-480-6565; E-mail: nishizus@mail.nih.gov

Mathematical simulations of the p53–Mdm2 feedback loop suggest that both proteins will exhibit impulsive expression characteristics in response to high cellular stress levels. However, little quantitative experimental evaluation has been performed, particularly of the phosphorylated forms. To evaluate the mathematical models experimentally, we used lysate microarrays from an isogenic pair of gamma ray–irradiated cell lysates from HCT116 (*p53*$^{+/+}$ and *p53*$^{-/-}$). Both p53 and Mdm2 proteins showed expected pulses in the wild type, whereas no pulses were seen in the knockout. Based on experimental observations, we determined model parameters and generated an *in silico* 'knockout', reflecting the experimental data, including phosphorylated proteins.

Biological responses in cells are coordinated by signaling networks based on protein dynamics. A major goal in the elucidation of biological networks is to develop mathematical models of the dynamics of protein signaling pathways. However, mathematical modeling of such pathways is limited by the lack of an appropriate, high-throughput means to experimentally validate protein dynamics under different experimental conditions. For instance, the instantaneous state of a biological network will vary according to both the type of stimulus and the time of measurement. Therefore, acquiring quantitative information from different conditions or time points is extremely important for model development and validation. To achieve the monitoring of multi-dimensional (different conditions, times, and proteins) pathway dynamics, a study format allowing the simultaneous measurement of many proteins across many samples is ideal. 'Reverse-phase' protein lysate microarrays (RPAs) have been developed for quantitative proteomic monitoring in various biological contexts (1, 2). In principle, the RPA technique involves spotting whole-cell-fraction lysates in a microarray format to detect particular proteins with specific primary antibodies, making it especially useful when testing many samples in a single experiment.

Using RPA technology, we captured the protein dynamics of the p53–Mdm2 feedback loop, one of the best-studied biological networks. An important tumor suppressor protein, p53, is mutated frequently in human cancers, and is vital to cell mechanisms such as DNA repair, apoptosis, and cell cycle regulation. As a key transcriptional regulator, p53 binds to specific sequences in DNA and activates many downstream genes, including *Mdm2*. In turn, the Mdm2 protein inhibits the transcriptional activity of p53 and enhances its degradation. This negative feedback loop

keeps the p53 protein level low yet stable under normal conditions and helps to switch off p53 at the end of a stress response. Accumulating knowledge of the p53–Mdm2 feedback mechanism has led investigators to explore mathematical methods to better understand this system (3-6). However, validating the plausibility of the mathematical models has not been a trivial task because of the many samples that are required from many time-points and the difficulty in quantitative protein monitoring in a high-throughput fashion. In the present study, we produced a high-density RPA from a p53-knockout model cell line, HCT116, to validate mathematical models of the p53–Mdm2 feedback loop by quantitative protein monitoring.

Materials and Methods

Cell culture. An isogenic pair of HCT116 colon cancer cell lines was kindly provided by Dr. Bert Vogelstein (Johns Hopkins University, Baltimore, MD) (7). Cells were grown at 37 °C in the presence of 5% CO_2 in McCoy's 5A medium containing 10% Fetal Bovine Serum.

Collection of cell lysate. The isogenic pair of HCT116 with three biological replicates were grown and collected independently. Following exposure to 0.3, 3, and 30 Gy of gamma irradiation using the ^{137}Cs Mark 1 irradiator (Shepard & Associates, San Francisco, CA), protein lysates of $p53^{+/+}$ and $p53^{-/-}$ at 10 time points over an 8-hour period were collected with a modified cell lysis protocol (1).

'Reverse-phase' protein lysate microarrays. The Aushon 2470 microarrayer (Aushon BioSystems, Burlington, MA) was used to produce the RPAs for this study. The array surface was a nitrocellulose-coated glass slide for which manufacturing conditions were optimized for our RPA (Grace BioLabs, Bend, OR). A set of nineteen 384-well microplates, each containing 10-time, 2-fold serial dilutions of each sample, was prepared. The robustness of the array design was maximized by including two technical replicates for each biological replicate, as well as ensuring that no two biological replicates were spotted by the same pin.

Image processing. To acquire enough bit depth and pixels per feature, an optical flatbed scanner (Epson 4870, Epson America, Long Beach, CA) with the resolution set to 16-bit, 2400 dpi was used. To prevent the image intensity from being skewed, a Wedge Density Strip (Danes-Picta, Praha, Czech Republic) was used for readout range calibration (8). The resulting images were processed by P-SCAN and Proteinscan software packages written in MATLAB.

Immunocytochemistry. A half-million cells were plated onto a cover glass and placed in a 3.5-cm Petri dish to grow on the surface of both the cover glass and the Petri dish. After 16–24 hours of incubation, the irradiated cells were processed for immunostaining with either mouse anti-p53 primary antibody (LabVision, Fremont, CA) or rabbit anti-p53-Ser15 antibody (Cell Signaling Technology, Danvers, MA), followed by fluorophore conjugated either with anti-mouse or with -rabbit IgG secondary antibodies.

Mathematical models. The premise of our model comes from the systems developed by Lev Bar-Or *et al*. and Ma *et al*. (5, 6). MATLAB (MathWorks, Natick, MA) language was used to program all simulations. The feedback loop circuits were divided into *Oscillator* and *Stress* modules. All equations and parameter settings are available in Supplemental Information.

Results

Quantitative monitoring of p53 and Mdm2 proteins. Since the wild-type cells ($p53^{+/+}$) have functional p53 activity, comparison with the knockout cells ($p53^{-/-}$) provides useful p53-dependent information about cellular response to DNA damage. To examine the p53-mediated stress response, protein lysates from each cell line were collected at 10 time points during a period of eight hours following exposure to ionizing radiation, at doses of 0.3, 3, and 30 Gy, and subjected to RPA production (Fig. 1*A*).

In $p53^{+/+}$ cells at a dose of 30 Gy, both proteins showed discrete peaks at approximately 4 and 7 hours (Fig. 1*B, C*). Oscillations of p53 and Mdm2 have been reported in computational simulations, with a delay caused by the time lag necessary for activation of Mdm2 by p53 (4-6); however, the discrete timing of our sample collections may have made this delay difficult to see. Evidence of a delay is better seen at the 2-hour time point in $p53^{+/+}$ cells exposed to 30 Gy, when p53 has begun to rise; however, Mdm2 does not increase until later. Mdm2 showed very little increase in $p53^{-/-}$ cells at all doses, suggesting involvement of p53 for Mdm2 induction after irradiation. Interestingly, $p53^{-/-}$ cells showed a gradual decrease in Mdm2 upon exposure to radiation, presumably due to

an increased rate of degradation. Thus, although $p53^{-/-}$ cells do not possess the p53 gene, p53-independent activity upstream of Mdm2 may still regulate Mdm2 stability (9, 10). In addition to stabilizing p53 by preventing Mdm2 from binding, phosphorylation at Ser15 is known to aid p53's ability to transcriptionally activate other genes (Fig. 1*D,E*) (11). Within the first hour following a high dose of radiation, the level of p53-Ser15 in $p53^{+/+}$ cells rises more rapidly than total p53, implying that phosphorylation of the existing cellular pool of p53 is critical for its accumulation after stress. Total Mdm2 falls (Fig. 1*C*) at all doses within the first hour after radiation, probably because of stress-induced degradation of Mdm2; however, Mdm2-Ser166 rises or stays constant, indicating that this form of the molecule might be more stable (Fig. 1*E*) (12). Phosphorylation of Mdm2 at Ser166 by ionizing radiation has been shown by inducing PKB/Akt activation, which presumably stabilizes Mdm2 and helps it enter the nucleus, where it inactivates p53 (12). Our observations of phosphorylated proteins with total p53 and Mdm2 levels indicate a possible correlation between phosphorylation at certain sites, conferring stability and activity of these species in this time period.

Mathematical models of the p53–Mdm2 feedback loop. The initial model generated by Lev Bar-Or *et al.* (5) showed damped oscillations of p53 and Mdm2 after stress through a mathematical representation of an unknown intermediary process leading to a delay in the p53-dependent induction of Mdm2. Recently, a model was developed by Ma *et al.* (6) depicting oscillations by showing the role of the DNA damage sensor, ATM, in both phosphorylating p53 and increasing the degradation of Mdm2 (13, 14). Based on these two studies, we generated an interaction map consisting of four proteins—p53,

Mdm2, p53-Ser15, and Mdm2-Ser166 (Fig. 2*A*). It should also be noted that other models have been shown to generate similar oscillations (15). For example, the model by Ciliberto *et al.* (4) showed oscillations of p53 as a result of both negative and positive feedback loops. Chikaramane *et al.* (3) proposed a model taking into account the role of additional proteins, including Arf, Siah, and B-Catenin in p53 regulation.

Our experimental results guided the assignment of parameter values for the set of differential equations (Supplemental Information), and notably of phosphorylated protein species. We fixed the time scale and the frequency of pulses of each protein to fit accordingly. Kinetic parameters were adjusted in the simulations of $p53^{+/+}$ cells until we observed oscillations of p53 and Mdm2 at approximately 4 and 7 hours to coincide with our experimental results (Fig. 3*A*). After making the appropriate parameter settings for p53 and Mdm2, peaks were seen in simulations of both p53 and p53-Ser15 at approximately 4 and 7 hours. As in our experiments, the level of p53-Ser15 rose more rapidly than that of total p53 within the first hour after stress was applied. Since the model incorporates the effect of upstream kinase activity on Mdm2, which induces rapid and selective degradation of the molecule, the simulations showed an initial dip in total Mdm2 level, consistent with simulations by others (4, 6) and with our RPA results. In contrast, we saw Mdm2-Ser166 stay at the initial level within the first 3 hours before exhibiting oscillations similar to our experimental observations, suggesting that phosphorylation at this site could prevent rapid degradation, thereby stabilizing the molecule (12).

Based on parameters that agreed with the RPA results in $p53^{+/+}$ cells, we created an *in silico* "knockout" of the p53 gene by setting the p53 production rate of the

mathematical models to zero (Fig. 3*B*). As in our experiments, total Mdm2 fell after exposure to stress, while Mdm2-Ser166 increased briefly up to 1 hour and decreased gradually afterwards. Interestingly, Mdm2 and Mdm2-Ser166 are similar in both $p53^{-/-}$ and $p53^{+/+}$ cells within the first 3 hours—total Mdm2 drops, and Mdm2-Ser166 is sustained. However, due to the lack of p53 production, total Mdm2 does not increase after 3 hours in $p53^{-/-}$ cells. This finding suggests that, after 3 hours, upstream kinase activity continues to degrade un-phosphorylated Mdm2, causing the Mdm2-Ser166 equilibrium to shift towards de-phosphorylation, which results in a concomitant decrease in Mdm2-Ser166 levels (Fig. 2*B*).

Protein expression synchronization in cell population. From our RPA results at lower radiation doses, we found that $p53^{+/+}$ cells appeared to show no noticeable oscillation. However, previous studies have shown that individual cells respond with discrete pulses in a nonsynchronized manner, even at low radiation doses (16). To explain this discrepancy, we stained populations of cells for p53 and p53-Ser15 expression after radiation at doses of 0.3, 3, and 30.0 Gy. We found more cells expressed higher levels of p53 in response to higher doses or radiation (**Fig. 4**). At lower doses, fewer cells may need to respond to DNA damage, presumably because the dose does not reach a threshold level necessary for a response in a majority of cells (17). Therefore, pulses at lower doses may not be clearly visible at the full population level due to an averaging effect. We postulate that, at higher doses, most cells respond at closer–to-maximum capacity, exhibiting pulses that are closely synchronized and therefore detectable at the full population level. These observations suggest that protein expression

kinetics at lower stress levels may not appropriately reflect the network at the single-cell level; however, at high stress levels, where most cells are showing response above the threshold level, population-driven quantitative data can still provide a reasonable approximation of the average stress-induced response of individual cells (17).

Discussion

Although successful mathematical modeling of signal transduction has been reported, details of the timing of events are largely missing because compensating quantitative experimental systems are lacking. The aims of our present study are: (i) to provide highly quantitative measurements at the protein level as a function of time; (ii) to simulate a gene knockout effect by mathematical modeling; and (iii) to compare the *in silico* knockout model with an isogenic *in vitro* model. Although we are not explicitly incorporating all of the existing identified molecules in the pathway as part of the equations, using a combination of the RPA system and the knockout isogenic cell lines, we predicted the knockout effect *in vitro* with an *in silico* approach at the protein level, suggesting that the robust response of the feedback loop represented by p53 and Mdm2 is consistent, although it may be a consequence of complex processes.

Molecular network studies often focus on signaling events by using averaged or pooled samples from a heterogeneous population. These data can be easily misinterpreted because individual cells behave differently in response to external stimuli. For instance, recent extensive protein imaging analysis revealed considerable variability of the p53–Mdm2 feedback loop at the single-cell level when cells were exposed to low and medium doses of γ irradiation (15). However, tracking multiple species of molecules with multiple

parameters at the single-cell level is not always feasible. Although a high-stress dose may be necessary to synchronize responses of the cells, using RPAs can be an adequate complementary technique to imaging analysis. Accumulating such quantitative proteomic reference data represents a substantial contribution to understanding signaling networks at the systems level.

ACKNOWLEDGMENTS

We thank Drs. Myong-Hee Sung and Toni Holway for critical discussions and reading of the manuscript, and Dr. Bert Vogelstein for providing HCT116 isogenic pair of cell lines. This project has been funded in whole or in part with federal funds from the National Cancer Institute, National Institutes of Health, under Contract N01-CO-12400. The content of this publication does not necessarily reflect the views or policies of the Department of Health and Human Services, nor does mention of trade names, commercial products, or organizations imply endorsement by the U.S. Government.

Figure Legends

Figure 1. | Protein expression dynamics measured by RPA. **(*A*)** The RPA slides stained with p53 and Mdm2 antibody are shown. The slides depict 3,800 features showing 10-time 2-fold serial dilutions and 2-time technical replicates of 190 different samples.

The 190 samples consist of protein lysates taken from 10 control samples, and 3 biological replicates of the 10 time points studied after the exposure of 2 cell lines to 3 radiation doses. The serial dilutions were used to produce dilution curves to facilitate quantitation. **(*B*)** Protein expression levels of total p53; **(*C*)** total Mdm2; **(*D*)** p53–Ser15; and **(*E*)** Mdm2–Ser166, generated by a DI_{25} algorithm, are plotted as a function of time. Each protein has a set of data from three doses and a pair of isogenic cell lines ($p53^{+/+}$ and $p53^{-/-}$). Each data point represents the average of 3 biological and 2 technical replicates. Horizontal axis indicates time (hours), and vertical axis indicates protein expression levels in AU (arbitrary units), calculated by dividing each data point by the value representing the maximum staining intensity found on the array. Error bars represent the standard error of the mean.

Figure 2. | Schematic diagram of the p53–Mdm2 feedback loop. Red and blue ovals represent p53 and Mdm2 molecules, respectively. Gray ovals represent those not incorporated in the mathematical models explicitly, but likely to play important roles in the feedback loop (18-20). **(*A*)** Under normal conditions, p53, Mdm2, p53–Ser15, and Mdm2–Ser166 are maintained at a steady-state level. In response to cell stress, oscillations in these protein levels are triggered as a result of activation signals and upstream kinase activity. HAUSP expression is not influenced by DNA damage (20). Solid arrows indicate signal transduction and conversion of the molecules. Mdm2–Ser166 inhibits p53 activity. Dashed arrows illustrate de-phosphorylation. **(*B*)** In knockout cells, where there is no p53, continuous degradation of un-phosphorylated Mdm2 may drive the equilibrium of Mdm2–Ser166 toward de-phosphorylation.

Figure 3. | Mathematical simulations of the p53–Mdm2 feedback loop. Each column illustrates the protein expression levels of four protein species. From the left, **(*A*)** RPA data of $p53^{+/+}$ cells and the simulations of $p53^{+/+}$ cells; **(*B*)** RPA data of $p53^{-/-}$ cells and the simulations (*in silico* knockout) of $p53^{-/-}$ cells. Horizontal axes indicate time (hours), and vertical axes indicate protein expression levels by linear scaled DI_{25} values (RPA results) and fold changes in concentration (simulations). The insets in **(*B*)** display the identical kinetics at the same scale as the wild type. Error bars represent the standard error of the mean.

Figure 4. | Expression of p53 and p53–Ser15 in response to different doses of ionizing radiation by immunochemistry in HCT116 $p53^{+/+}$ cells 4 hours after radiation. HCT116 $p53^{+/+}$ cells carry wild-type p53 alleles, and thus show visible basal levels of p53 staining in control (non-irradiated) cells. At 0.3 Gy, cells start responding by exhibiting p53, although most cells exhibit the same level of expression as the control. At 3.0 Gy, more cells show a distinct response than at 0.3Gy, but there is considerable heterogeniety. At 30 Gy, most cells show a distinct response. High-level expression is seen at 30 Gy, including some very high responders that are presumably pulsating. Expression of p53–Ser15 is also distinct at the dose of 30 Gy, although a small fraction of cells shows a visible response at lower doses. DAPI staining highlights the corresponding nuclear DNA. Error bars represent the standard error of the mean.

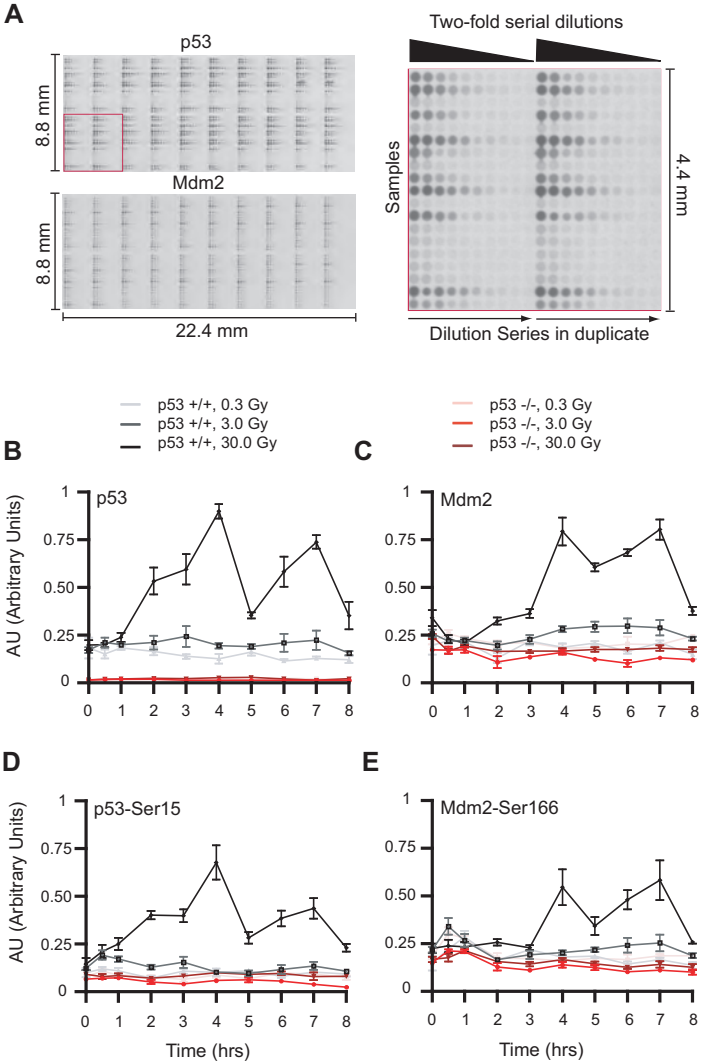
A
p53
8.8 mm
Mdm2
8.8 mm
22.4 mm
Two-fold serial dilutions
Samples
4.4 mm
Dilution Series in duplicate
p53 +/+, 0.3 Gy
p53 +/+, 3.0 Gy
p53 +/+, 30.0 Gy
p53 -/-, 0.3 Gy
p53 -/-, 3.0 Gy
p53 -/-, 30.0 Gy
B
p53
C
Mdm2
D
p53-Ser15
E
Mdm2-Ser166
AU (Arbitrary Units)
Time (hrs)

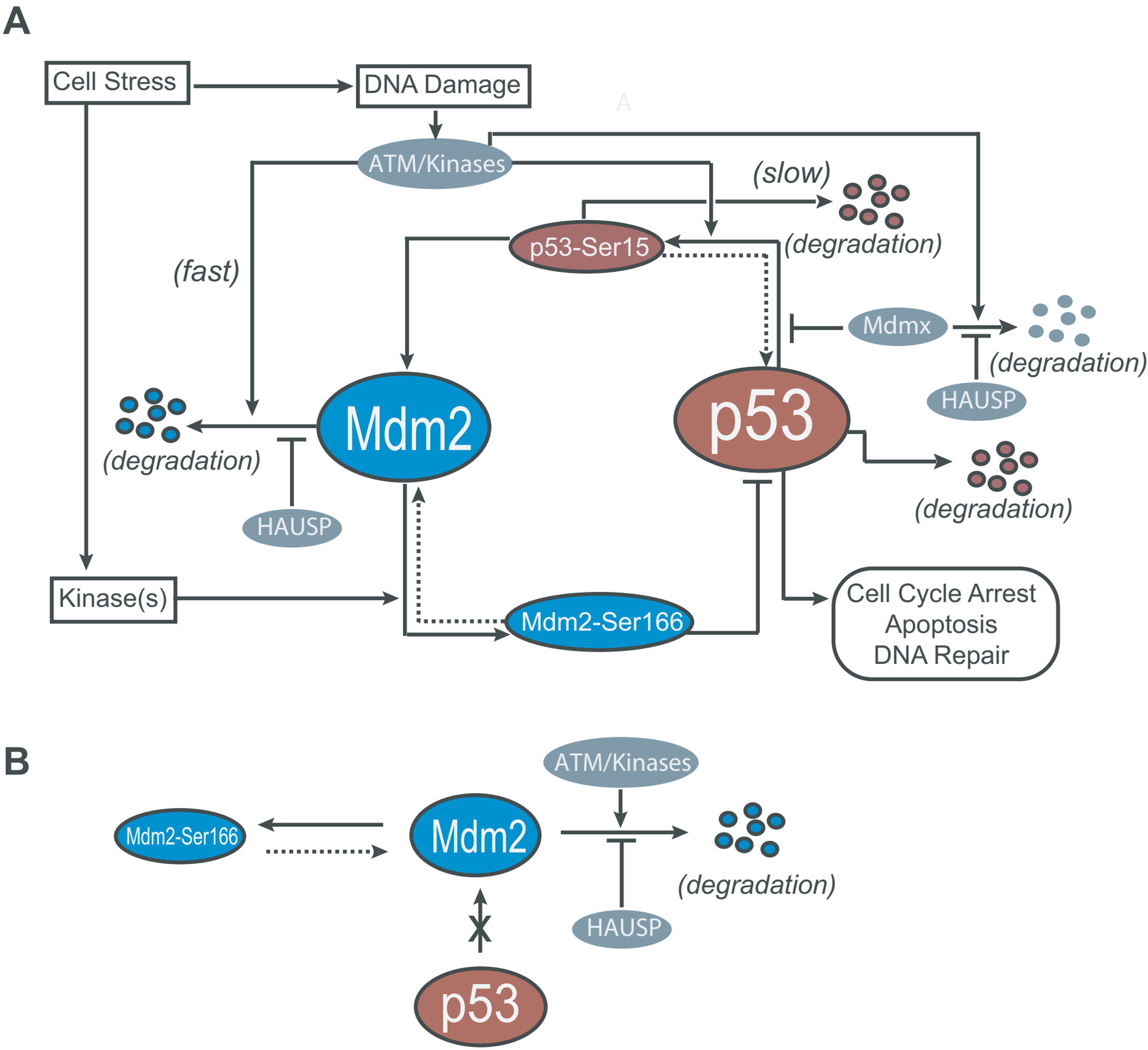
A
Cell Stress
DNA Damage
ATM/Kinases
(slow)
(degradation)
p53-Ser15
(fast)
Mdmx
(degradation)
HAUSP
Mdm2
p53
(degradation)
HAUSP
(degradation)
Kinase(s)
Mdm2-Ser166
Cell Cycle Arrest
Apoptosis
DNA Repair
B
ATM/Kinases
Mdm2-Ser166
Mdm2
(degradation)
HAUSP
p53

Fig. 2

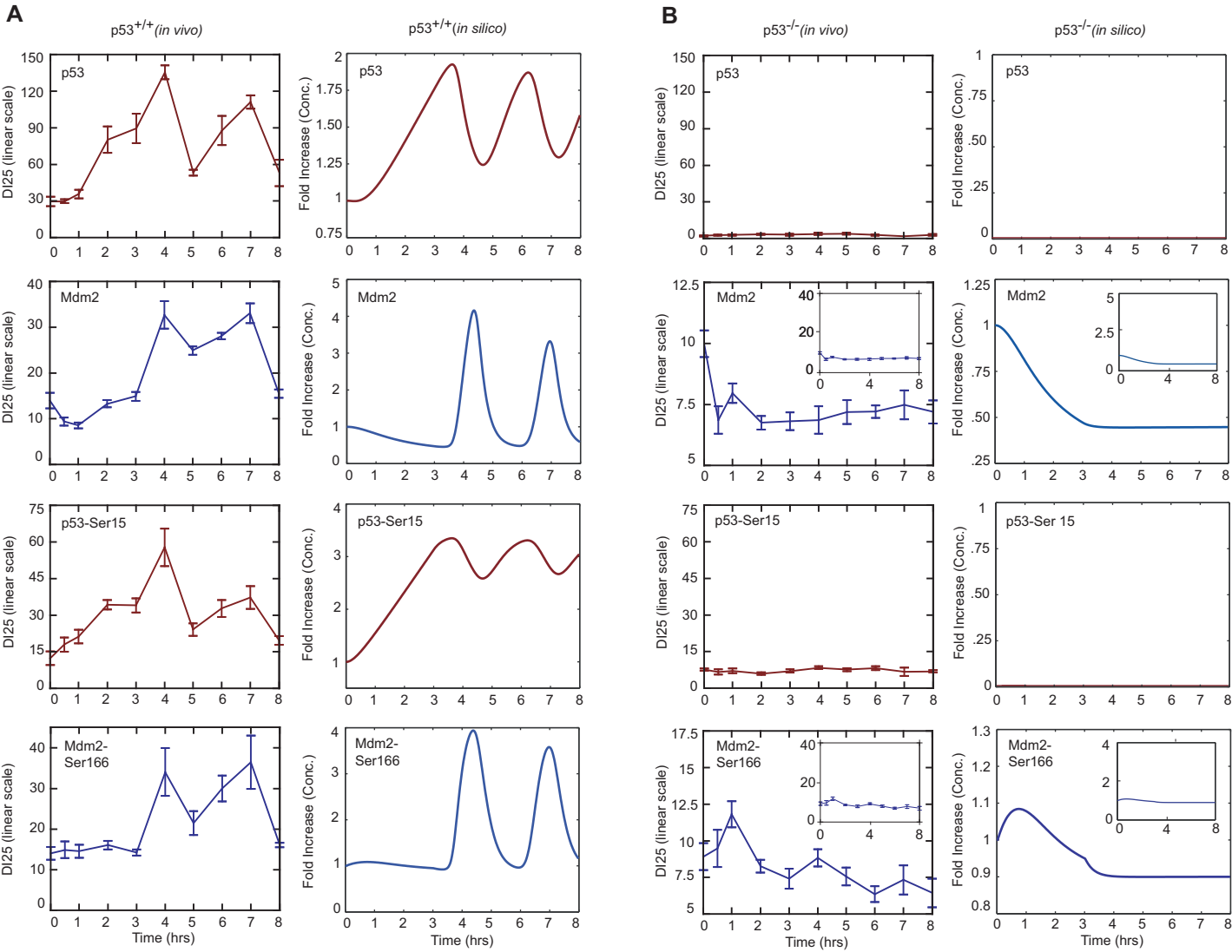
A
p53+/+(in vivo)
p53+/+(in silico)
B
p53-/-(in vivo)
p53-/-(in silico)
p53
Mdm2
p53-Ser15
Mdm2-Ser166
p53-Ser 15
DI25 (linear scale)
Fold Increase (Conc.)
Time (hrs)

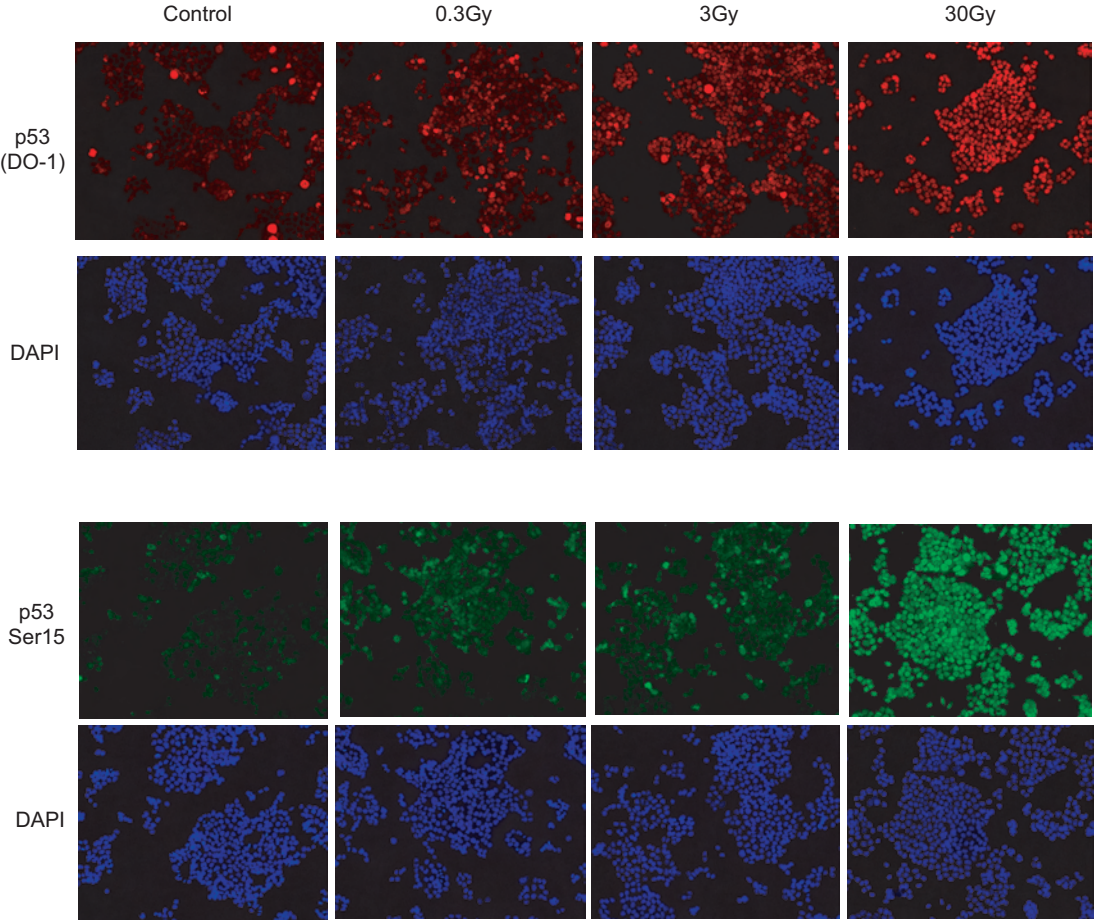

Fig. 4